

## Research Article

# Synthesis of CuO/Co<sub>3</sub>O<sub>4</sub> Coaxial Heterostructures for Efficient and Recycling Photodegradation

R. X. Chen,<sup>1</sup> S. L. Zhu,<sup>1,2</sup> J. Mao,<sup>1,2</sup> Z. D. Cui,<sup>1</sup> X. J. Yang,<sup>1,2</sup> Y. Q. Liang,<sup>1,2</sup> and Z. Y. Li<sup>1,2</sup>

<sup>1</sup>School of Materials Science and Engineering, Tianjin University, Tianjin 300072, China

<sup>2</sup>Tianjin Key Laboratory of Composite and Functional Materials, Tianjin 300072, China

Correspondence should be addressed to S. L. Zhu; slzhu@tju.edu.cn and Y. Q. Liang; yqliang@tju.edu.cn

Received 16 September 2015; Revised 2 November 2015; Accepted 4 November 2015

Academic Editor: Wanjun Wang

Copyright © 2015 R. X. Chen et al. This is an open access article distributed under the Creative Commons Attribution License, which permits unrestricted use, distribution, and reproduction in any medium, provided the original work is properly cited.

The highly efficient CuO/Co<sub>3</sub>O<sub>4</sub> composite photocatalyst with different morphologies has been synthesized directly on Cu wire mesh by controlling the composition of cobalt-containing solid precursors via a simple hydrothermal method. The structure morphology and composition of the composite photocatalyst have been characterized by scanning electron microscopy (SEM), transmission electron microscopy (TEM), X-ray diffraction (XRD), X-ray photoelectron spectroscopy (XPS), and UV-visible diffuse reflectance spectra. The photocatalytic result shows that the CuO/Co<sub>3</sub>O<sub>4</sub> coaxial heterostructure is easy to recycle and exhibit enhanced photodegradation activity for methylene blue compared to single CuO nanorod arrays under full spectrum solar light irradiation. The enhanced photocatalytic efficiency of the composite could be ascribed to the synergistic effect of CuO and Co<sub>3</sub>O<sub>4</sub>. This study provides a general and effective method in the fabrication of 1D composition NRs with sound heterojunctions that show enhancement of photocatalytic performance and facility of recycling.

## 1. Introduction

Organic dyes, which are widely used in various industrial processes, form an integral part of industrial wastewater. Photocatalytic degradation of organic pollutants by semiconductor photocatalysts is promising for environmental purification and energy conversion [1–5], because it has been successfully employed to treat a wide range of toxic and nondegradable organic pollutants into readily biodegradable compounds in the wastewater without involving complex technologies [6–10].

Nevertheless, most of the widely used photocatalysts have two main limitations: one is the low solar energy conversion efficiency due to their wide band gap and the high recombination ratio of photoinduced electron-hole pairs, and the other is the difficulties of the catalysts' recycling. Therefore, seeking highly active photocatalysts which are easy to recycle is still an intensifying endeavor worldwide. One-dimensional (1D) nanostructures including nanorods (NRs), nanowires (NWs), nanotubes (NTs), and nanofibers (NFs) have drawn particular attention because of their high specific surface area and facility of electronic transmission [11, 12].

Therefore, many oxides with 1D nanostructures have been widely used as catalysts in photocatalytic reactions. However, photocatalysis, in general, is blamed for the low quantum yields caused by the electron/hole recombination. For further improvement of photocatalytic activity, the p-n, n-n, and p-p junctions formed in combination with both p-type and n-type semiconductors can effectively reduce the recombination rate of photogenerated electro/hole pairs, which subsequently enhances the photocatalytic activity [13, 14]. 1D nanowire (NW) heterostructures grown directly on conductive substrate are of great interest because of their large surface areas, efficient electron transfer, fast ion transport, easy electrolyte access to electrode, and good strain accommodation [15–18].

CuO, as a p-type semiconductor with a narrow band gap (1.2 eV in bulk), is one of the most prominent catalysts and is extensively used in environmental catalysis. Spinel cobalt tetroxide (Co<sub>3</sub>O<sub>4</sub>) is a compound of CoO and Co<sub>2</sub>O<sub>3</sub> with rich oxygen content and thus also exhibits p-type semiconducting properties. In this study, we presynthesized CuO NRs array grown directly on Cu wire mesh via thermal oxidation and the synthesis of Co<sub>3</sub>O<sub>4</sub> nanostructures with

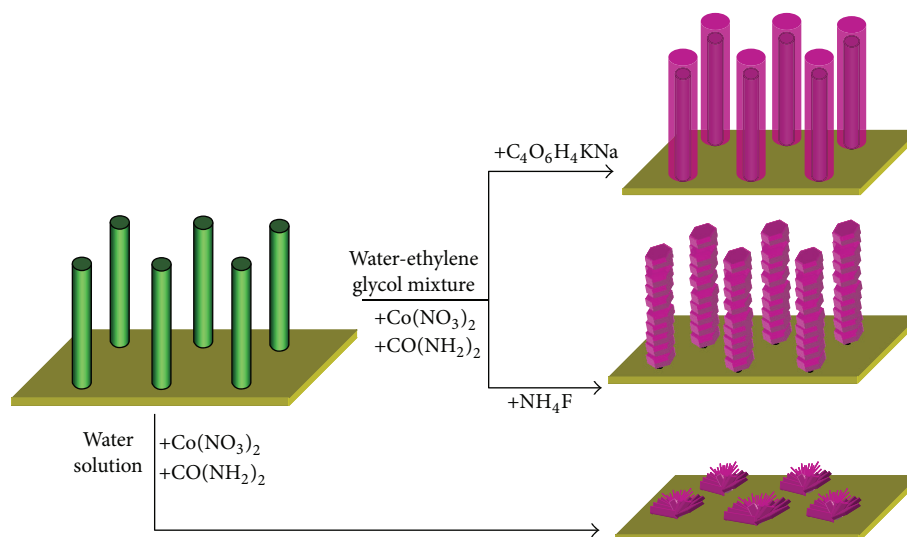


FIGURE 1: Schematic illustration of different morphologies of CuO/Co<sub>3</sub>O<sub>4</sub> composites.

different morphologies by simple and effective hydrothermal method at relatively low temperature on CuO NRs arrays. These hybrid nanostructures were aligned on Cu substrates, which can directly serve as a physical support of these structures. Thus, the photocatalysts can be easily recycled after photocatalytic reactions. Compared with the single CuO NRs and Co<sub>3</sub>O<sub>4</sub> nanoflowers, the composite exhibits a potential synergistic effect with remarkably enhanced photocatalytic performances in terms of MB degradation.

## 2. Experimental

### 2.1. Sample Preparation

**2.1.1. Growth of CuO NRs.** All chemicals (purity of 99.9%) used in this research were of analytical purity and used without further purification. CuO NR arrays were synthesized on copper mesh using a simple and low cost thermal oxidation method as reported before [19–21]. First, small pieces (9 cm<sup>2</sup>) of Cu mesh were cut and cleaned by acetone, ethanol, and water, 5 minutes in each, consecutively and finally rinsed with DI water and dried with air blowing. Then, the Cu mesh was immediately transferred into an open furnace and annealed under air at 500°C for 2 hours. After cooling down to room temperature, a dense array of copper oxide NRs was obtained on copper mesh.

**2.1.2. Synthesis of Co<sub>3</sub>O<sub>4</sub>/CuO Composite.** CuO/Co<sub>3</sub>O<sub>4</sub> composite was produced by a hydrothermal growth method. CuO/Co<sub>3</sub>O<sub>4</sub> coaxial heterostructures: 0.07 M cobaltous nitrate (Co(NO<sub>3</sub>)<sub>2</sub>·6H<sub>2</sub>O) was dissolved in 30 mL mixture solution of ethylene glycol and water (15 mL:15 mL). 0.04 M Seignette salt (C<sub>4</sub>O<sub>6</sub>H<sub>4</sub>KNa) and 0.36 M urea (CO(NH<sub>2</sub>)<sub>2</sub>) were introduced in the solution above subsequently. CuO/Co<sub>3</sub>O<sub>4</sub> nanosheets: 0.07 M cobaltous nitrate (Co(NO<sub>3</sub>)<sub>2</sub>·6H<sub>2</sub>O) was dissolved in 30 mL mixture solution of ethylene glycol and water (15 mL:15 mL). 0.14 M

ammonium fluoride (NH<sub>4</sub>F) and 0.36 M urea (CO(NH<sub>2</sub>)<sub>2</sub>) were introduced in the solution above subsequently. Co<sub>3</sub>O<sub>4</sub> nanoflowers: 0.07 M cobaltous nitrate (Co(NO<sub>3</sub>)<sub>2</sub>·6H<sub>2</sub>O) and 0.36 M urea (CO(NH<sub>2</sub>)<sub>2</sub>) were dissolved in 30 mL deionized water. The solutions were then transferred to Teflon-lined stainless steel autoclave and the copper mesh with CuO NRs was immersed in this solution. The autoclave was maintained at 90°C for 5 hours. After natural cooling, the copper meshes with CuO NRs were removed from the autoclave and washed multiple times with distilled water and then dried in air. Subsequently, the as-synthesized Co<sub>3</sub>O<sub>4</sub>/CuO composites were calcined at 350°C for 2 hours. There were three kinds of CuO/Co<sub>3</sub>O<sub>4</sub> composites that were synthesized in the hydrothermal growth process as shown in Figure 1.

**2.2. Sample Characterization.** The surface morphology and structure of samples were characterized by field emission scanning electron microscopy (FE-SEM, Hitachi S-4800), X-ray diffraction (XRD, RIGAKU/DMAX), and transmission electron microscopy (TEM, Philips Tecnai G2 F20). Surface chemical analysis of CuO/Co<sub>3</sub>O<sub>4</sub> coaxial heterostructures was performed by X-ray photoelectron spectroscopy (XPS) using a PHL1600ESCA instrument equipped with a monochromatic Mg Ka X-ray source ( $E = 1253.6$  eV) operating at 250 W. The Raman spectra were collected by using DXR Microscope (Thermo Electron Corporation). Room temperature photoluminescence (PL) spectra were recorded using Jobin Yvon Fluorolog-3-21 spectrofluorometer equipped with Xe lamp (excitation wavelength = 325 nm). Nitrogen adsorption isotherms of the CuO NRs and Co<sub>3</sub>O<sub>4</sub>/CuO composites were measured at 77 K using an autosorb iQ instrument (Quantachrome, USA). The total surface was calculated from the Brunauer-Emmett-Teller (BET) method and the pore size distribution data was calculated using the Barrett-Joyner-Halenda (BJH) method based on the adsorption and desorption data.

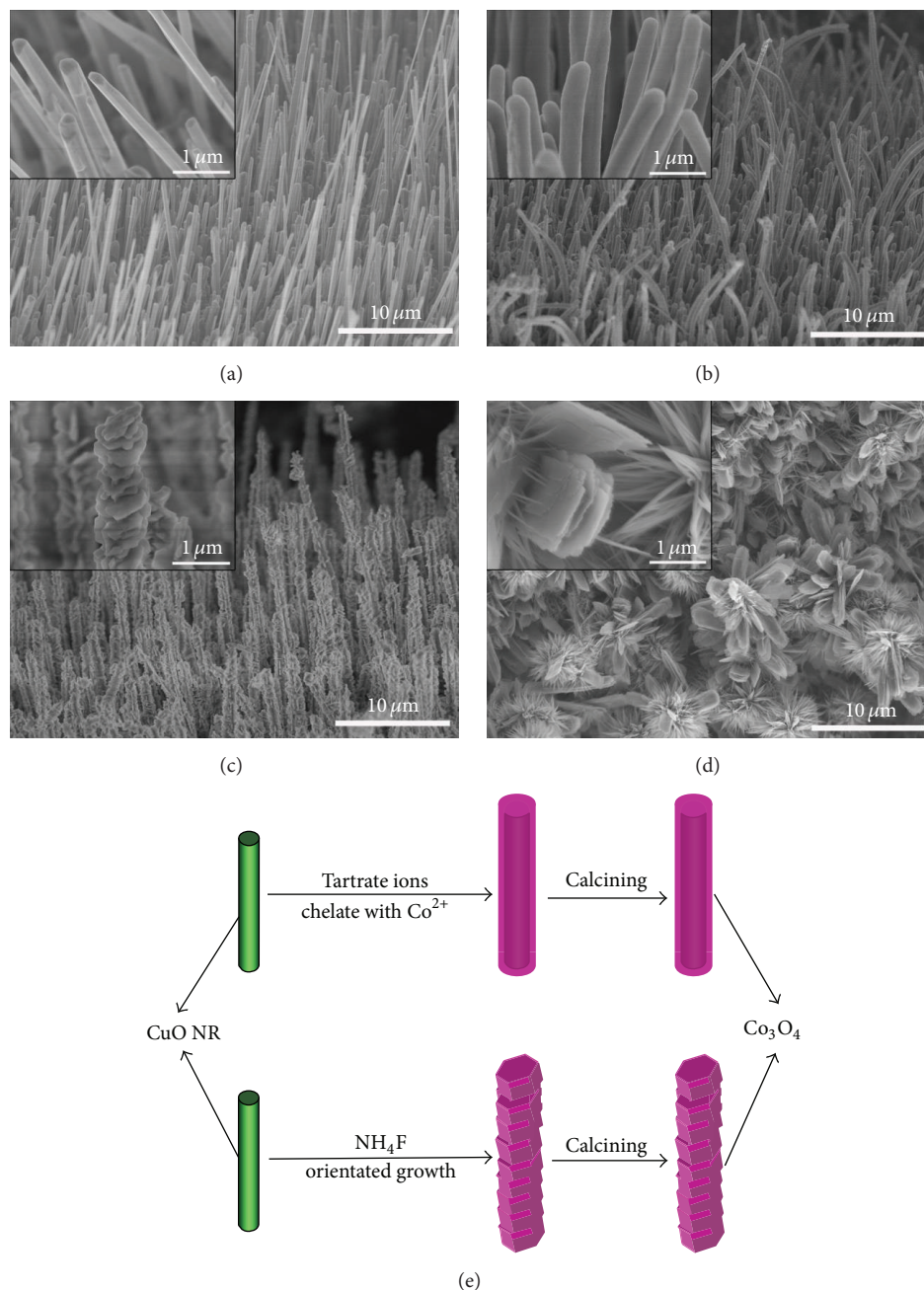


FIGURE 2: SEM images of (a) CuO NR arrays and different morphology of CuO/Co<sub>3</sub>O<sub>4</sub> composite, (b) CuO/Co<sub>3</sub>O<sub>4</sub> coaxial heterostructures, (c) CuO/Co<sub>3</sub>O<sub>4</sub> nanosheets, and (d) Co<sub>3</sub>O<sub>4</sub> nanoflowers. The insets show the high-magnification images of the corresponding samples. (e) Schematic diagram of the growth mechanism of the CuO/Co<sub>3</sub>O<sub>4</sub> composite photocatalyst.

**2.3. Photocatalytic Activity.** Degradation of methylene blue was used to evaluate the photocatalytic activity of Co<sub>3</sub>O<sub>4</sub>/CuO composites. The methylene blue without photocatalysts was designed as the blank control experiment. A little piece (9 cm<sup>2</sup>) of copper mesh with CuO NRs and Co<sub>3</sub>O<sub>4</sub>/CuO composites was put in a 50 mL of aqueous solution with methylene blue concentration of 10 mg/L. In order to establish an adsorption/desorption equilibrium, the solution was stirred in the dark for 30 min. A 500 W Xenon lamp was served as the light source. The residual

concentration of methylene blue was evaluated by ultraviolet-visible (UV-Vis) spectrometry.

### 3. Results and Discussion

**3.1. Morphology and Structure.** The morphology of Co<sub>3</sub>O<sub>4</sub>/CuO composites was studied by SEM as shown in Figure 2. The Co<sub>3</sub>O<sub>4</sub>/CuO composites were developed on the basis of CuO NRs arrays, which are composed of vertically arranged CuO nanorods with the diameter of 100 nm and

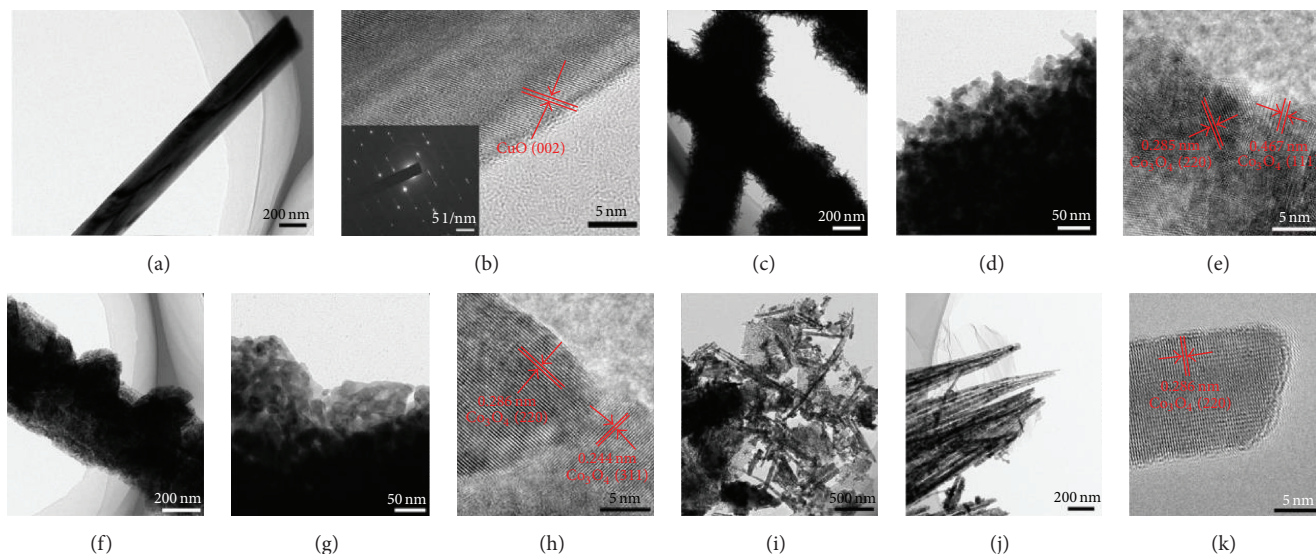


FIGURE 3: TEM/HRTEM images of CuO NR (a) and (b), (c–e) for CuO/Co<sub>3</sub>O<sub>4</sub> coaxial heterostructures, (f–h) for CuO/Co<sub>3</sub>O<sub>4</sub> nanosheets, and (i–k) for Co<sub>3</sub>O<sub>4</sub> nanoflowers.

the length of 4–10  $\mu\text{m}$  (Figure 2(a)). Figure 2(b) shows the SEM image of CuO/Co<sub>3</sub>O<sub>4</sub> coaxial heterostructures after a typical hydrothermal treatment and annealing. It is observed that the CuO NRs were fully covered by Co<sub>3</sub>O<sub>4</sub>. We can conclude from the inset high-magnification image that the surfaces of the nanowires are smooth and the diameter of CuO/Co<sub>3</sub>O<sub>4</sub> coaxial heterostructures is about 350 nm which is apparent larger than CuO NRs. The morphology of CuO/Co<sub>3</sub>O<sub>4</sub> nanosheet is observed in Figure 2(c). Many pieces of nanosheets neatly covered CuO NRs and the diameter increases to about 400 nm. Figure 2(d) shows the microstructure of Co<sub>3</sub>O<sub>4</sub> nanoflowers which are mainly composed of Co<sub>3</sub>O<sub>4</sub> nanosheets and nanoneedles but the CuO NRs cannot be found.

The formation mechanism of Co<sub>3</sub>O<sub>4</sub> nanostructures could be proposed as follows (Figure 2(e)). According to our previous work [22], there will be two kinds of cobalt-containing solid precursors: cobalt oxide acetate (C<sub>8</sub>H<sub>12</sub>Co<sub>3</sub>O<sub>9</sub>) and cobalt acetate hydrate (C<sub>4</sub>H<sub>6</sub>CoO<sub>4</sub>·4H<sub>2</sub>O). The Co<sub>3</sub>O<sub>4</sub> grains were obtained by calcining the precursors which will react with oxygen to produce Co<sub>3</sub>O<sub>4</sub>, water, and carbon dioxide. Urea in these reactions served mainly as a source for the generation of both ammonia cations and hydroxyl anions. The tartrate ions which are generated by adding Seignette salt will chelate with divalent cobalt cations and enwrap the CuO NRs, thus forming CuO/Co<sub>3</sub>O<sub>4</sub> coaxial heterostructures [22]. The wall-like, organized, hierarchical structures will be obtained with the presence of NH<sub>4</sub>F which is used to provide ammonia cations [23]. The absence of ethylene glycol will make the CuO NRs broken, and the Co<sub>3</sub>O<sub>4</sub> nanoflower will be grown separately on the Cu substrate; see Figure 2(d). Further experiments are needed to illustrate the specific growth mechanism.

TEM image of a single CuO NR is shown in Figure 3(a), exhibiting a diameter of 200 nm. The single-crystalline nature of CuO NR is exhibited by the high-resolution TEM (HRTEM) image (Figure 3(b)). The calculated lattice spacing is about 0.25 nm corresponding to (002) plane of monoclinic CuO, which is consistent with that reported elsewhere for the CuO NRs synthesized with the same method [24]. The CuO/Co<sub>3</sub>O<sub>4</sub> coaxial heterostructures were dispersed in ethanol and analyzed by TEM, as shown in Figures 3(c)–3(e). The CuO/Co<sub>3</sub>O<sub>4</sub> coaxial heterostructures are covered by numerous interconnected Co<sub>3</sub>O<sub>4</sub> nanoparticles with an average diameter of 10 nm. In the crystallography, both (220) planes with a lattice spacing of 0.285 nm and (111) planes with a lattice spacing of 0.467 nm were observed.

The TEM image shown in Figures 3(f) and 3(g) indicates that the CuO/Co<sub>3</sub>O<sub>4</sub> nanosheets are composed of numerous Co<sub>3</sub>O<sub>4</sub> nanoparticles. The diameter of each Co<sub>3</sub>O<sub>4</sub> nanoparticle is about 20 nm. The HRTEM was employed to further characterize the Co<sub>3</sub>O<sub>4</sub> nanoparticle. As can be seen from Figure 3(h), the nanoparticles are linked together and the lattice fringes with a lattice spacing of about 0.286 and 0.244 nm correspond to (220) and (311) planes.

The panoramic morphology of the Co<sub>3</sub>O<sub>4</sub> nanoflowers is shown in Figure 3(i). The Co<sub>3</sub>O<sub>4</sub> nanoflowers disintegrated into layers and needles during the ultrasonic in alcohol. It can be clearly observed from Figure 3(j) that the Co<sub>3</sub>O<sub>4</sub> nanoneedle consisted of many Co<sub>3</sub>O<sub>4</sub> nanoparticles with a typical diameter of about 20 nm. Figure 3(k) shows an HRTEM image recorded near the edge of the Co<sub>3</sub>O<sub>4</sub> nanoneedle. The fringe spacing of about 0.286 nm corresponds to the (220) plane.

The XRD pattern (Figure 4) reveals the crystal structure and phase purity of the CuO NR and CuO/Co<sub>3</sub>O<sub>4</sub> coaxial heterostructures. The XRD pattern of CuO NRs (red line in

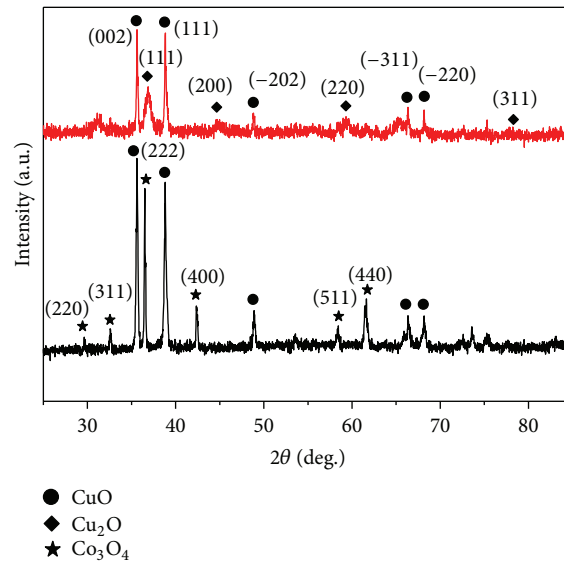


FIGURE 4: XRD patterns of as-prepared CuO NRs and CuO/Co<sub>3</sub>O<sub>4</sub> coaxial heterostructures.

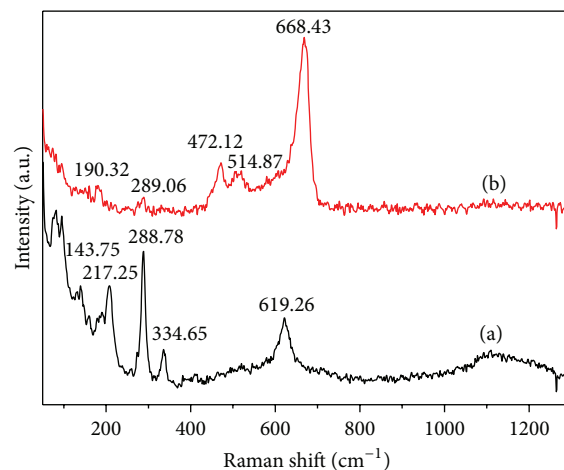


FIGURE 5: Raman spectra of CuO NRs (a) and CuO/Co<sub>3</sub>O<sub>4</sub> coaxial heterostructures (b).

Figure 4) can be indexed to the monoclinic CuO (JCPDS number 43-1004) and the hexagonal phase of Cu<sub>2</sub>O (JCPDS number 05-0667). All Co<sub>3</sub>O<sub>4</sub> diffraction peaks are clearly seen in the black line and match very well with those of face-centered cubic Co<sub>3</sub>O<sub>4</sub> phase of spinel cobalt oxide with a lattice constant of  $a = 8.084 \text{ \AA}$  (JCPDS number 09-0418).

In addition, the formation of Co<sub>3</sub>O<sub>4</sub> crystal was also confirmed by Raman spectra, as depicted in Figure 5. The wavenumbers were observed at around 289, 334, and 619 cm<sup>-1</sup>, all of which belong to Ag and Bg modes of CuO [25–27]. Two weak characteristic peaks at about 143 and 217 cm<sup>-1</sup> for the Cu<sub>2</sub>O structures are observed in the Raman spectrum [28, 29]. The band at approximately 191 cm<sup>-1</sup> was ascribed to the  $F_{2g}$  mode of Co<sub>3</sub>O<sub>4</sub> [30, 31]. The bands with medium intensity located at approximately 472 and 514 cm<sup>-1</sup> were corresponding to the  $E_g$  and  $F_{2g}$  symmetry modes, respectively. The band positioned at 668 cm<sup>-1</sup> is close to the

11g peaks of Co<sub>3</sub>O<sub>4</sub> [32, 33]. In fact, the Raman spectra of the CuO/Co<sub>3</sub>O<sub>4</sub> coaxial heterostructures show a combination of the characteristic bands of CuO and Co<sub>3</sub>O<sub>4</sub>.

Figure 6 illustrates the further XPS measurements for the CuO NRs and CuO/Co<sub>3</sub>O<sub>4</sub> coaxial heterostructures. The survey spectrum of CuO NRs shows only peaks corresponding to Cu and O, while the spectrum corresponding to the CuO/Co<sub>3</sub>O<sub>4</sub> coaxial heterostructures shows the peaks corresponding to Cu, O, and Co. The Cu 2p spectrum of the CuO NRs was shown in the Figure 6(a). XPS analysis illustrates that copper oxides are present in two oxidation states, Cu<sup>2+</sup> in cupric oxide (CuO) and Cu<sup>1+</sup> in cuprous oxide (Cu<sub>2</sub>O). The band at a binding energy of 934.3, 942.4 eV, and 961.7 eV corresponds to Cu 2p<sub>1/2</sub> and Cu 2p<sub>3/2</sub> in CuO. The bands at 952.2, 932.3, and 963.2 eV correspond to Cu 2p<sub>1/2</sub> and Cu 2p<sub>3/2</sub> in Cu<sub>2</sub>O [34, 35]. Figure 6(b) shows the spectrum of O of the CuO NRs. The present O 1s spectrum at 529.9 eV belongs to the CuO, and the O 1s peak at 531.7 eV

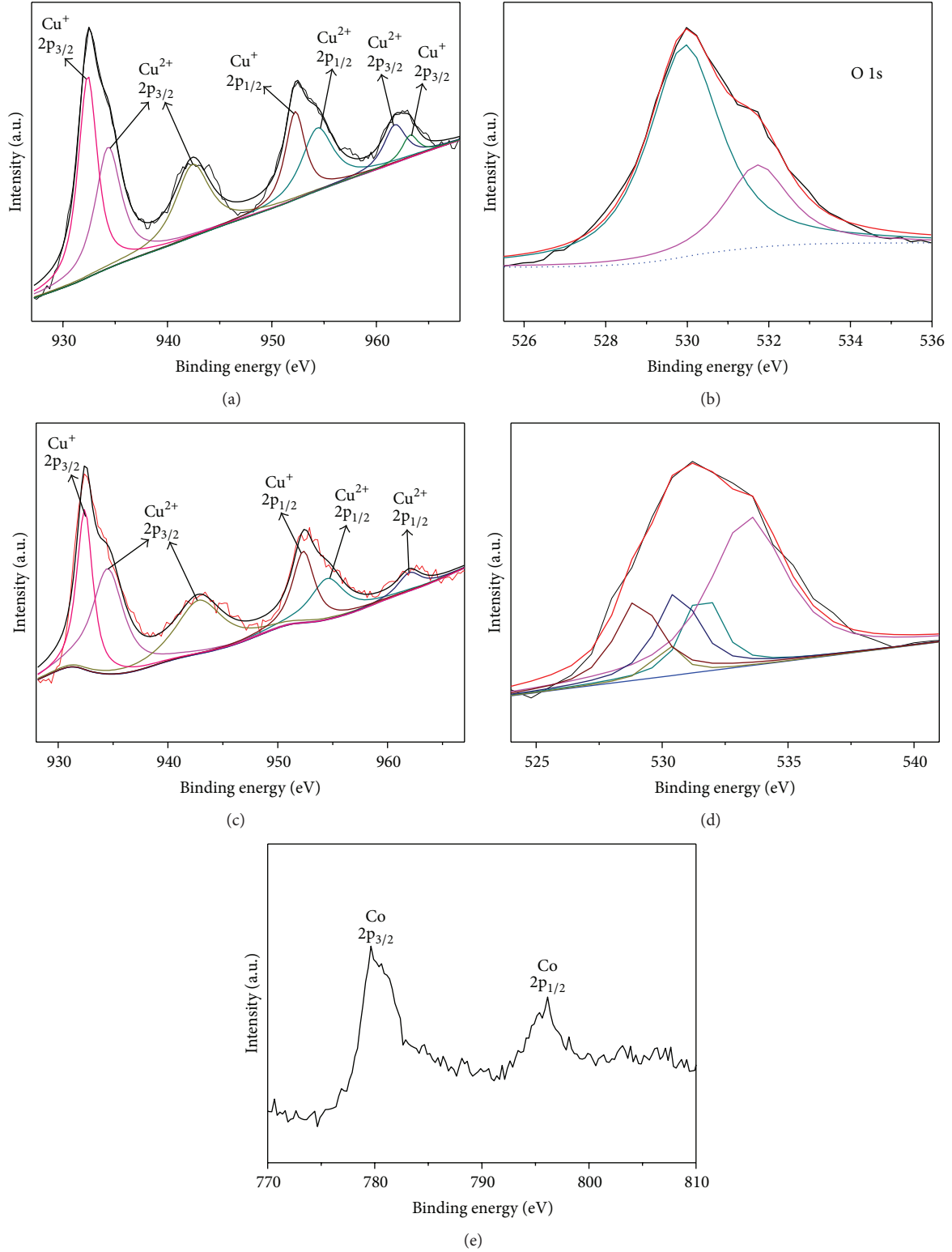


FIGURE 6: XPS spectra of (a) Cu 2p, (b) O 1s for CuO NRs, (c) Cu 2p, and (d) O 1s for CuO/Co<sub>3</sub>O<sub>4</sub> coaxial heterostructures. (e) XPS spectra of Co 2p for CuO/Co<sub>3</sub>O<sub>4</sub> coaxial heterostructures.

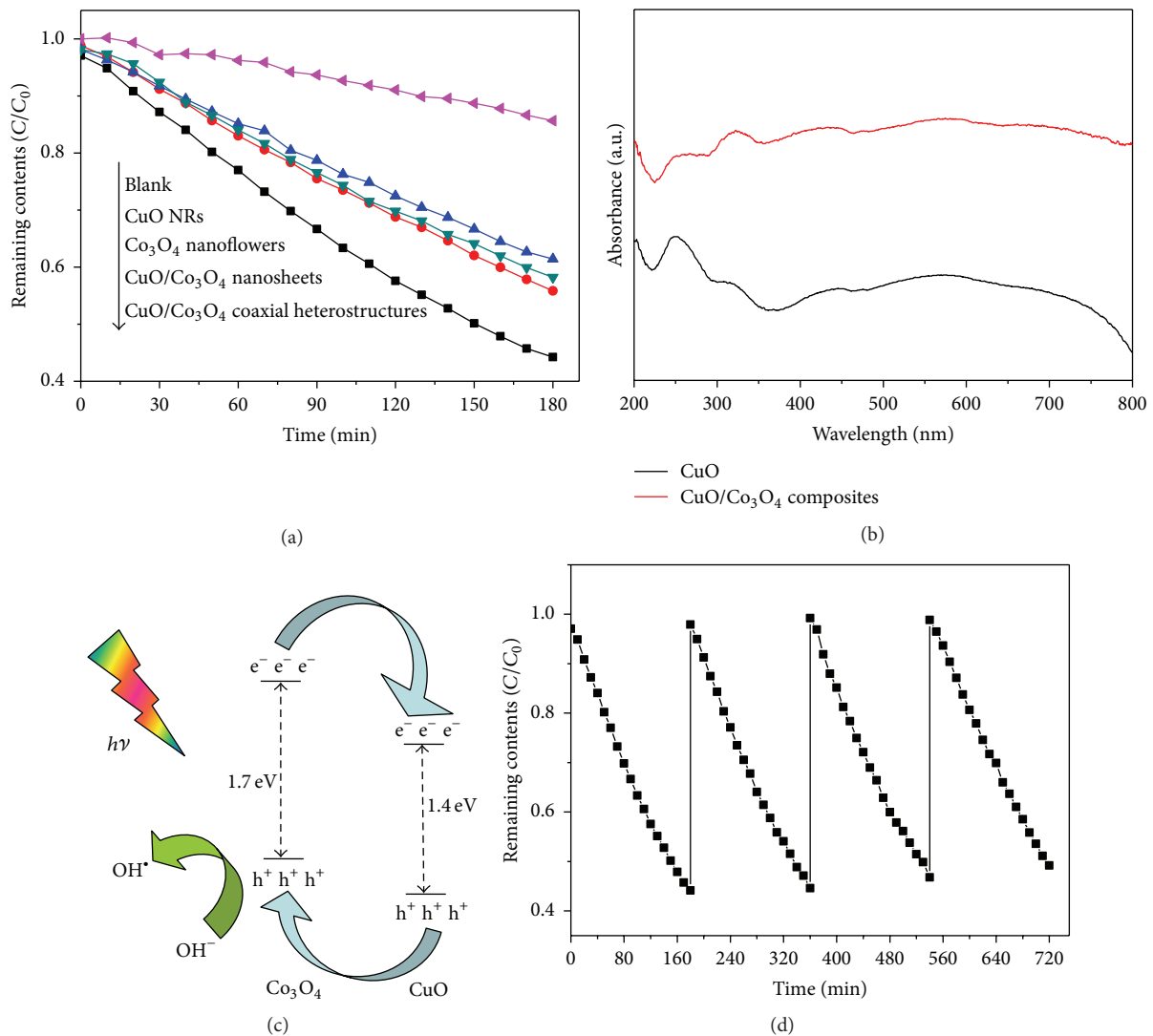


FIGURE 7: (a) Comparison of photocatalytic activities of bare CuO NRs and CuO/Co<sub>3</sub>O<sub>4</sub> composites for the photocatalytic decolorization of MB in water. (b) UV-Vis absorption spectra of CuO NRs and CuO/Co<sub>3</sub>O<sub>4</sub> coaxial heterostructures. (c) Proposed charge separation for CuO/Co<sub>3</sub>O<sub>4</sub> coaxial heterostructures under light irradiation. (d) Cycling degradation curves for CuO/Co<sub>3</sub>O<sub>4</sub> coaxial heterostructures.

is due to the absorption of the O atom in the Cu<sub>2</sub>O [36]. The Cu 2p spectrum of the CuO/Co<sub>3</sub>O<sub>4</sub> coaxial heterostructures (Figure 6(c)) is similar to that of the CuO NRs. O 1s spectra of CuO/Co<sub>3</sub>O<sub>4</sub> coaxial heterostructures were deconvoluted into five peaks (Figure 6(d)). The peaks at 529.2 eV and 530.6 eV are attributed to lattice oxygen in CuO and Cu<sub>2</sub>O. The peak located at 530.2 eV is attributed to the lattice oxygen in Co<sub>3</sub>O<sub>4</sub> [22, 37]. The peaks which were found at 531.6 and 533.4 eV imply the existence of Co-OH and H<sub>2</sub>O molecules [38, 39].

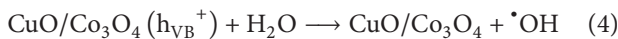
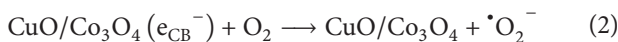
The Co 2p<sub>3/2</sub> and Co 2p<sub>1/2</sub> main peaks are located at 780.8 and 797.0 eV (shown in Figure 6(e)), which is approximately the same as the standard spectrum of Co<sub>3</sub>O<sub>4</sub> [22, 40].

**3.2. Photocatalysis.** The photocatalytic degradation of MB dye on CuO/Co<sub>3</sub>O<sub>4</sub> composites was carried out under full spectrum solar light irradiation. The blank test was carried

out to determine the contribution of photolysis of MB. Under the full spectrum solar light irradiation in a period of 180 minutes, self-degradation of MB is about 15% of the original organic MB dye under irradiation. Both CuO NRs and Co<sub>3</sub>O<sub>4</sub> nanoflowers show apparent photocatalytic activity for the MB degradation, while limited improvements were observed by combining the two semiconductors in the sample of CuO/Co<sub>3</sub>O<sub>4</sub> nanosheets. It is clear to see that large amount of Co<sub>3</sub>O<sub>4</sub> grains is accumulated on CuO NRs, and the grain boundaries of Co<sub>3</sub>O<sub>4</sub> particles would impede electronic transfers in CuO/Co<sub>3</sub>O<sub>4</sub> nanosheets. Therefore, the photocatalytic performance of CuO/Co<sub>3</sub>O<sub>4</sub> nanosheets was not improved dramatically. However, CuO/Co<sub>3</sub>O<sub>4</sub> coaxial heterostructures exhibit highest photocatalytic activity among the four samples. After irradiation for 180 minutes, the CuO/Co<sub>3</sub>O<sub>4</sub> coaxial heterostructures are able to degrade

about 56% of the original organic MB dye, while the degradation rate of CuO NRs is only about 40% (Figure 7(a)).

The enhanced photocatalytic performance of CuO/Co<sub>3</sub>O<sub>4</sub> composite can mainly be explained by the electron-hole (e-h) charge separation which results in the synergism and coupling effect between the two semiconductors. The conduction band (CB) and valence band (VB) potentials of Co<sub>3</sub>O<sub>4</sub> and CuO can be calculated based on the previous literatures [41, 42]. Semiconductors could use the irradiation light which corresponds to the band gap to make valence band electron excited to the conduction band while creating a hole in the valence band. Compared with CuO NRs, the CuO/Co<sub>3</sub>O<sub>4</sub> coaxial heterostructures show stronger capability of light absorption (Figure 7(b)). There was a wide peak at around 250–400 nm which indicates that the CuO/Co<sub>3</sub>O<sub>4</sub> coaxial heterostructures increase the coefficient of light utilization. The band structure of the heterostructures permits the transfer of electrons from CB of Co<sub>3</sub>O<sub>4</sub> to CB of CuO and transfer of holes from VB of CuO to VB of Co<sub>3</sub>O<sub>4</sub>, as shown in Figure 7(c). Therefore, the recombination of electron-hole pairs will be hindered and the photocatalytic property would be improved. The holes transferred to cobalt oxides are trapped by H<sub>2</sub>O and OH<sup>-</sup> to further produce <sup>•</sup>OH and OH<sup>-</sup> species. On the basis of this discussion, the proposed mechanisms in expression form are as follows:



The recycle experiments were conducted to evaluate the photostability of CuO/Co<sub>3</sub>O<sub>4</sub> coaxial heterostructures. Compared with powder, copper substrate can make the catalyst easy to recycle. After each cycle, we washed the CuO/Co<sub>3</sub>O<sub>4</sub> coaxial heterostructures with DI water and dried them in air and refreshed MB dye was added in the reactor. The degradation efficiencies at 180 minutes of CuO/Co<sub>3</sub>O<sub>4</sub> coaxial heterostructures photocatalyst were in sequence of 44.15%, 44.59%, 46.79%, and 49.2% (Figure 7(d)). Results showed that the changing trend of degradation efficiency of the sample was almost the same as the fresh CuO/Co<sub>3</sub>O<sub>4</sub> coaxial heterostructures. The recycle experiments indicate that the CuO/Co<sub>3</sub>O<sub>4</sub> coaxial heterostructures are sufficiently stable and do not exhibit any significant loss after four terms of recycling; thus, it has potentially practical applications in treating contaminated water.

In order to examine the efficiency of charge carrier trapping, immigration, and transfer, as well as understanding the fate of e<sup>-</sup>/h<sup>+</sup> pairs in semiconductor particles, the CuO

NRs and Co<sub>3</sub>O<sub>4</sub>/CuO composites were subjected to photoluminescence (PL) measurements. The PL spectra of the samples are shown in Figure 8(a). The PL spectrum of the CuO NRs shows a broad emission band centered at 440 nm, which indicated CuO emission [43–45]. By contrast, the PL spectrum of the Co<sub>3</sub>O<sub>4</sub>/CuO composites samples shows much lower intensity, which indicates that the recombination of electron-hole pairs is restrained. Based on the above results, we can conclude that the Co<sub>3</sub>O<sub>4</sub>/CuO composites could act as an active center for hindering the rapid recombination of photoinduced electron-hole pairs, thus enhancing the photocatalytic performance. Figures 8(b)–8(d) show the N<sub>2</sub> adsorption-desorption isotherm of the CuO NRs and Co<sub>3</sub>O<sub>4</sub>/CuO composites. The Brunauer-Emmett-Teller (BET) specific surface area calculated from N<sub>2</sub> isotherms at 77 K of the CuO NRs, CuO/Co<sub>3</sub>O<sub>4</sub> coaxial heterostructures, and CuO/Co<sub>3</sub>O<sub>4</sub> nanosheets is 6.386 m<sup>2</sup> g<sup>-1</sup>, 3.526 m<sup>2</sup> g<sup>-1</sup>, and 3.979 m<sup>2</sup> g<sup>-1</sup>, respectively. In addition, the pore size distribution diagram (the inset) based on Barrett-Joyner-Halenda (BJH) method clearly indicates that pore is in the mesoporous region. The pore size distributions of the CuO NRs and CuO/Co<sub>3</sub>O<sub>4</sub> coaxial heterostructures are around 4 nm. However, the pore size of the CuO/Co<sub>3</sub>O<sub>4</sub> nanosheets increased to 9 nm. Notice that although the specific surface area of Co<sub>3</sub>O<sub>4</sub>/CuO composites is decreased compared to CuO NRs, the photocatalytic performance increases significantly. This indicates that the synergism and coupling effects between CuO and Co<sub>3</sub>O<sub>4</sub> play more dominant role than specific surface area of the catalysts in improving photocatalytic properties. It is noteworthy that CuO/Co<sub>3</sub>O<sub>4</sub> coaxial heterostructures and CuO/Co<sub>3</sub>O<sub>4</sub> nanosheets possess almost same specific surface area but different pore size distributions. The smaller pore size of CuO/Co<sub>3</sub>O<sub>4</sub> coaxial heterostructures may result in the higher photocatalytic activity than that of CuO/Co<sub>3</sub>O<sub>4</sub> nanosheets.

## 4. Conclusions

In summary, novel CuO/Co<sub>3</sub>O<sub>4</sub> coaxial heterostructures were prepared by hydrothermal methods. The morphology of composite strongly affects the efficiency of photodegradation. Compared with CuO NRs, CuO/Co<sub>3</sub>O<sub>4</sub> nanosheets, and Co<sub>3</sub>O<sub>4</sub> nanoflowers, the synthesized CuO/Co<sub>3</sub>O<sub>4</sub> coaxial heterostructures catalysts showed high photocatalytic efficiency for the degradation of MB under full spectrum solar light irradiation. The overlapping of band structure plays an important role in charge transfer and separation for high photocatalytic activity. Because of its stability and being easy to recycle, the CuO/Co<sub>3</sub>O<sub>4</sub> coaxial heterostructures are promising for practical application for water purification.

## Conflict of Interests

The authors declare that there is no conflict of interests regarding the publication of this paper.

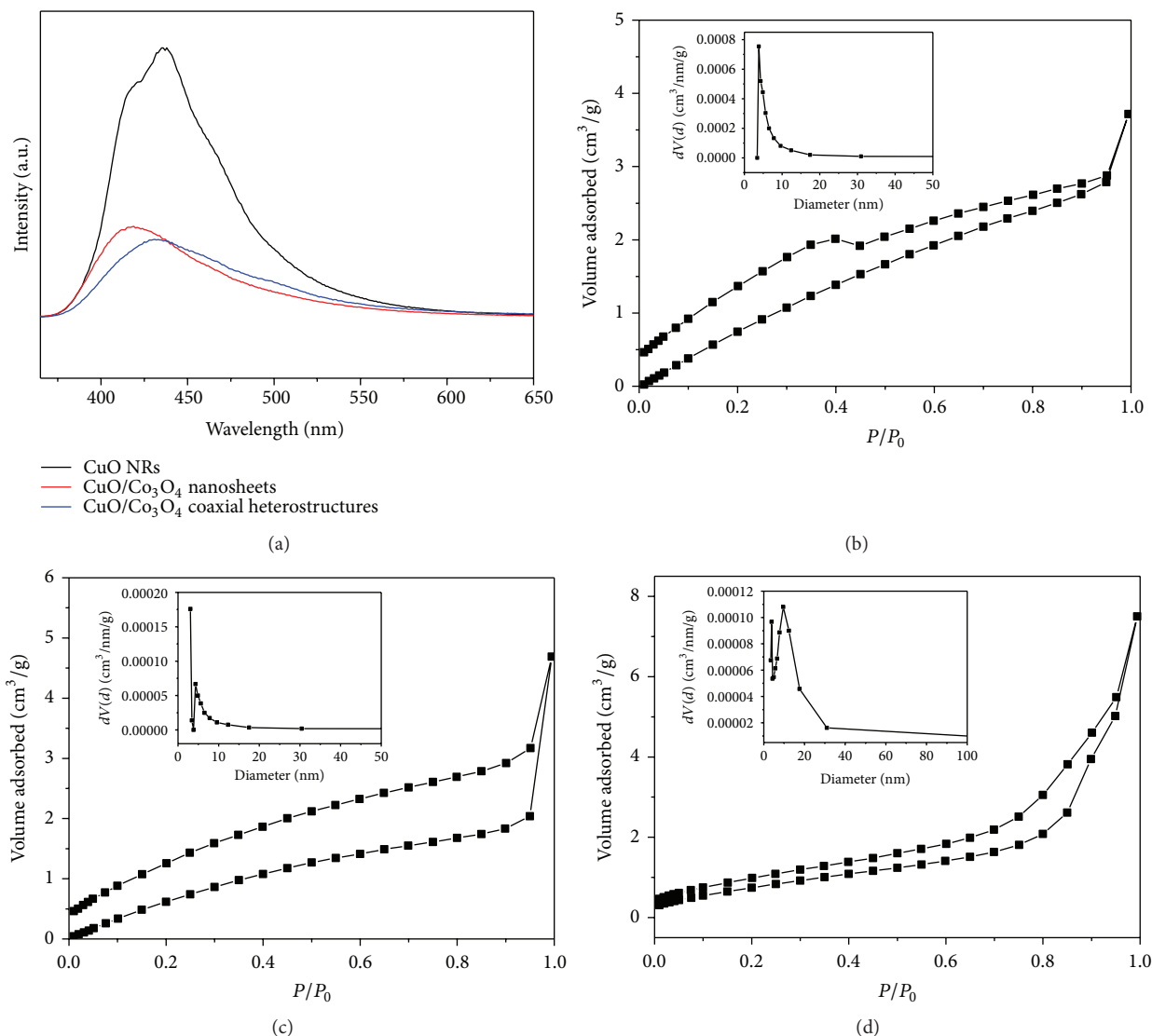


FIGURE 8: (a) The photoluminescence (PL) spectra of the CuO NRs, CuO/Co<sub>3</sub>O<sub>4</sub> coaxial heterostructures, and CuO/Co<sub>3</sub>O<sub>4</sub> nanosheets. Nitrogen adsorption-desorption isotherm for mesoporosity and BJH pore size distribution plot (inset): (b) CuO NRs; (c) CuO/Co<sub>3</sub>O<sub>4</sub> coaxial heterostructures; (d) CuO/Co<sub>3</sub>O<sub>4</sub> nanosheets.

## Acknowledgments

Financial supports by National Natural Science Foundation of China (51402211) and Natural Science Foundation of Tianjin (15JQJNC03600) are gratefully acknowledged.

## References

- [1] I. K. Konstantinou and T. A. Albanis, "TiO<sub>2</sub>-assisted photocatalytic degradation of azo dyes in aqueous solution: kinetic and mechanistic investigations: a review," *Applied Catalysis B: Environmental*, vol. 49, no. 1, pp. 1–14, 2004.
- [2] H. Tong, S. Ouyang, Y. Bi, N. Umezawa, M. Oshikiri, and J. Ye, "Nano-photocatalytic materials: possibilities and challenges," *Advanced Materials*, vol. 24, no. 2, pp. 229–251, 2012.
- [3] A. Houas, H. Lachheb, M. Ksibi, E. Elaloui, C. Guillard, and J.-M. Herrmann, "Photocatalytic degradation pathway of methylene blue in water," *Applied Catalysis B: Environmental*, vol. 31, no. 2, pp. 145–157, 2001.
- [4] S. Sakthivel, B. Neppolian, M. V. Shankar, B. Arabindoo, M. Palanichamy, and V. Murugesan, "Solar photocatalytic degradation of azo dye: comparison of photocatalytic efficiency of ZnO and TiO<sub>2</sub>," *Solar Energy Materials & Solar Cells*, vol. 77, no. 1, pp. 65–82, 2003.
- [5] N. Daneshvar, D. Salari, and A. R. Khataee, "Photocatalytic degradation of azo dye acid red 14 in water on ZnO as an alternative catalyst to TiO<sub>2</sub>," *Journal of Photochemistry & Photobiology A Chemistry*, vol. 162, no. 2-3, pp. 317–322, 2004.
- [6] S.-M. Lam, J.-C. Sin, A. Z. Abdullah, and A. R. Mohamed, "Degradation of wastewaters containing organic dyes photocatalysed by zinc oxide: a review," *Desalination & Water Treatment*, vol. 41, no. 1-3, pp. 131–169, 2012.
- [7] M. N. Chong, B. Jin, C. W. K. Chow, and C. Saint, "Recent developments in photocatalytic water treatment technology: a review," *Water Research*, vol. 44, no. 10, pp. 2997–3027, 2010.

- [8] Y. N. Tan, C. L. Wong, and A. R. Mohamed, "An overview on the photocatalytic activity of nano-doped-TiO<sub>2</sub> in the degradation of organic pollutants," *ISRN Materials Science*, vol. 2011, Article ID 261219, 18 pages, 2011.
- [9] Y. Zhang, M. K. Ram, E. K. Stefanakos, and D. Y. Goswami, "Synthesis, characterization, and applications of ZnO nanowires," *Journal of Nanomaterials*, vol. 2012, Article ID 624520, 22 pages, 2012.
- [10] S. Ahmed, M. G. Rasul, W. N. Martens, R. Brown, and M. A. Hashib, "Heterogeneous photocatalytic degradation of phenols in wastewater: a review on current status and developments," *Desalination*, vol. 261, no. 1-2, pp. 3-18, 2010.
- [11] X. Chen, Z. Li, J. Yang, Q. Sun, and S. Dou, "Aqueous preparation of surfactant-free copper selenide nanowires," *Journal of Colloid & Interface Science*, vol. 442, pp. 140-146, 2015.
- [12] C. Dong, X. Xiao, G. Chen, H. Guan, and Y. Wang, "Synthesis and photocatalytic degradation of methylene blue over p-n junction Co<sub>3</sub>O<sub>4</sub>/ZnO core/shell nanorods," *Materials Chemistry and Physics*, vol. 155, pp. 1-8, 2015.
- [13] M. Lee and K. Yong, "Highly efficient visible light photocatalysis of novel CuS/ZnO heterostructure nanowire arrays," *Nanotechnology*, vol. 23, no. 19, Article ID 194014, 2012.
- [14] X. Gao, Z. Wang, F. Fu, X. Li, and W. Li, "2D double-layer-tube-shaped structure Bi<sub>2</sub>S<sub>3</sub>/ZnS heterojunction with enhanced photocatalytic activities," *Physica B: Condensed Matter*, vol. 474, pp. 81-89, 2015.
- [15] G. Zhang, T. Wang, X. Yu, H. Zhang, H. Duan, and B. Lu, "Nanoforest of hierarchical Co<sub>3</sub>O<sub>4</sub>@NiCo<sub>2</sub>O<sub>4</sub> nanowire arrays for high-performance supercapacitors," *Nano Energy*, vol. 2, no. 5, pp. 586-594, 2013.
- [16] H. Wang, D. Ma, X. Huang, Y. Huang, and X. Zhang, "General and controllable synthesis strategy of metal oxide/TiO<sub>2</sub> hierarchical heterostructures with improved lithium-ion battery performance," *Scientific Reports*, vol. 2, article 701, 2012.
- [17] W. Zhou, C. Cheng, J. Liu et al., "Epitaxial growth of branched  $\alpha$ -Fe<sub>2</sub>O<sub>3</sub>/SnO<sub>2</sub> nano-heterostructures with improved lithium-ion battery performance," *Advanced Functional Materials*, vol. 21, no. 13, pp. 2439-2445, 2011.
- [18] X. Xia, J. Tu, Y. Zhang et al., "Porous hydroxide nanosheets on preformed nanowires by electrodeposition: branched nanoarrays for electrochemical energy storage," *Chemistry of Materials*, vol. 24, no. 19, pp. 3793-3799, 2012.
- [19] R. Mema, L. Yuan, Q. Du, Y. Wang, and G. Zhou, "Effect of surface stresses on CuO nanowire growth in the thermal oxidation of copper," *Chemical Physics Letters*, vol. 512, no. 1-3, pp. 87-91, 2011.
- [20] P. Raksa, A. Gardchareon, T. Chairuangri, P. Mangkornong, N. Mangkornong, and S. Choopun, "Ethanol sensing properties of CuO nanowires prepared by an oxidation reaction," *Ceramics International*, vol. 35, no. 2, pp. 649-652, 2009.
- [21] F. Wu, Y. Myung, and P. Banerjee, "Unravelling transient phases during thermal oxidation of copper for dense CuO nanowire growth," *CrystEngComm*, vol. 16, no. 16, pp. 3264-3267, 2014.
- [22] Y. Q. Liang, Z. D. Cui, S. L. Zhu et al., "Design of a highly sensitive ethanol sensor using a nano-coaxial p-Co<sub>3</sub>O<sub>4</sub>/n-TiO<sub>2</sub> heterojunction synthesized at low temperature," *Nanoscale*, vol. 5, no. 22, pp. 10916-10926, 2013.
- [23] F. Wu, X. Ma, J. Feng, Y. Qian, and S. Xiong, "3D Co<sub>3</sub>O<sub>4</sub> and CoO@C wall arrays: morphology control, formation mechanism, and lithium-storage properties," *Journal of Materials Chemistry A*, vol. 2, no. 30, pp. 11597-11605, 2014.
- [24] X. Jiang, T. Herricks, and Y. Xia, "CuO nanowires can be synthesized by heating copper substrates in air," *Nano Letters*, vol. 2, no. 12, pp. 1333-1338, 2002.
- [25] D. Chen, G. Shen, K. Tang, and Y. Qian, "Large-scale synthesis of CuO shuttle-like crystals via a convenient hydrothermal decomposition route," *Journal of Crystal Growth*, vol. 254, no. 1-2, pp. 225-228, 2003.
- [26] D. P. Volanti, D. Keyson, L. S. Cavalcante et al., "Synthesis and characterization of CuO flower-nanostructure processing by a domestic hydrothermal microwave," *Journal of Alloys and Compounds*, vol. 459, no. 1-2, pp. 537-542, 2008.
- [27] J. F. Xu, W. Ji, Z. X. Shen et al., "Preparation and characterization of CuO nanocrystals," *Journal of Solid State Chemistry*, vol. 147, no. 2, pp. 516-519, 1999.
- [28] M. Santamaria, G. Conigliaro, F. Di Franco, and F. Di Quarto, "Photoelectrochemical evidence of Cu<sub>2</sub>O/TiO<sub>2</sub> nanotubes hetero-junctions formation and their physicochemical characterization," *Electrochimica Acta*, vol. 144, pp. 315-323, 2014.
- [29] Y. Liu, W. Zhang, L. Bian, W. Liang, J. Zhang, and B. Yu, "Structure, morphology and photocatalytic activity of Cu<sub>2</sub>O/Pt/TiO<sub>2</sub> three-layered nanocomposite films," *Materials Science in Semiconductor Processing*, vol. 21, no. 1, pp. 26-32, 2014.
- [30] S. Deng, X. Xiao, X. Xing, J. Wu, W. Wen, and Y. Wang, "Structure and catalytic activity of 3D macro/mesoporous Co<sub>3</sub>O<sub>4</sub> for CO oxidation prepared by a facile self-sustained decomposition of metal-organic complexes," *Journal of Molecular Catalysis A: Chemical*, vol. 398, pp. 79-85, 2015.
- [31] K. Zhou, J. Liu, P. Wen, Y. Hu, and Z. Gui, "Morphology-controlled synthesis of Co<sub>3</sub>O<sub>4</sub> by one step template-free hydrothermal method," *Materials Research Bulletin*, vol. 67, pp. 87-93, 2015.
- [32] T. Cai, H. Huang, W. Deng, Q. Dai, W. Liu, and X. Wang, "Catalytic combustion of 1,2-dichlorobenzene at low temperature over Mn-modified Co<sub>3</sub>O<sub>4</sub> catalysts," *Applied Catalysis B: Environmental*, vol. 166-167, pp. 393-405, 2015.
- [33] L. Khalil, C. Eid, M. Bechelany, N. Abboud, A. Khoury, and P. Miele, "Design of CoFe<sub>2</sub>O<sub>4</sub>/Co<sub>3</sub>O<sub>4</sub> nanofibers with tunable morphology by Electrospinning," *Materials Letters*, vol. 140, pp. 27-30, 2015.
- [34] U. Arellano, J. M. Shen, J. A. Wang et al., "Dibenzothiophene oxidation in a model diesel fuel using CuO/GC catalysts and H<sub>2</sub>O<sub>2</sub> in the presence of acetic acid under acidic condition," *Fuel*, vol. 149, pp. 15-25, 2015.
- [35] Y. Wang, F. Qu, J. Liu, Y. Wang, J. Zhou, and S. Ruan, "Enhanced H<sub>2</sub>S sensing characteristics of CuO-NiO core-shell microspheres sensors," *Sensors and Actuators B: Chemical*, vol. 209, pp. 515-523, 2015.
- [36] S. C. Vanithakumari, S. L. Shinde, and K. K. Nanda, "Controlled synthesis of CuO nanostructures on Cu foil, rod and grid," *Materials Science and Engineering B: Solid-State Materials for Advanced Technology*, vol. 176, no. 8, pp. 669-678, 2011.
- [37] R. Xu and H. C. Zeng, "Self-generation of tiered surfactant superstructures for one-pot synthesis of Co<sub>3</sub>O<sub>4</sub> nanocubes and their close-and non-close-packed organizations," *Langmuir*, vol. 20, no. 22, pp. 9780-9790, 2004.
- [38] J. Yang, H. Liu, W. N. Martens, and R. L. Frost, "Synthesis and characterization of cobalt hydroxide, cobalt oxyhydroxide, and cobalt oxide nanodiscs," *The Journal of Physical Chemistry C*, vol. 114, no. 1, pp. 111-119, 2010.
- [39] W. Zhang, Y. Li, S. Zhu, and F. Wang, "Influence of argon flow rate on TiO<sub>2</sub> photocatalyst film deposited by dc reactive magnetron sputtering," *Surface and Coatings Technology*, vol. 182, no. 2-3, pp. 192-198, 2004.
- [40] M. Long, W. Cai, J. Cai, B. Zhou, X. Chai, and Y. Wu, "Efficient photocatalytic degradation of phenol over Co<sub>3</sub>O<sub>4</sub>/BiVO<sub>4</sub>

- composite under visible light irradiation,” *Journal of Physical Chemistry B*, vol. 110, no. 41, pp. 20211–20216, 2006.
- [41] B. J. Hansen, N. Kouklin, G. Lu, I.-K. Lin, J. Chen, and X. Zhang, “Transport, analyte detection, and opto-electronic response of p-type CuO nanowires,” *The Journal of Physical Chemistry C*, vol. 114, no. 6, pp. 2440–2447, 2010.
- [42] Y. Sun, J.-Y. Yang, R. Xu, L. He, R.-F. Dou, and J.-C. Nie, “Evidence for surface states in a single 3 nm diameter  $\text{Co}_3\text{O}_4$  nanowire,” *Applied Physics Letters*, vol. 96, no. 26, Article ID 262106, 2010.
- [43] İ. Y. Erdoğan and Ö. Güllü, “Optical and structural properties of CuO nanofilm: its diode application,” *Journal of Alloys and Compounds*, vol. 492, no. 1-2, pp. 378–383, 2010.
- [44] Y. Wang, T. Jiang, D. Meng, H. Jin, and M. Yu, “Controllable fabrication of nanowire-like CuO film by anodization and its properties,” *Applied Surface Science*, vol. 349, pp. 636–643, 2015.
- [45] B. Toboongsunga and P. Singjaia, “Formation of CuO nanorods and their bundles by an electrochemical dissolution and deposition process,” *Journal of Alloys and Compounds*, vol. 509, no. 10, pp. 4132–4137, 2011.



**Hindawi**

Submit your manuscripts at  
<http://www.hindawi.com>

